Nanoscale

ROYAL SOCIETY OF CHEMISTRY

PAPER

View Article Online
View Journal | View Issue

Cite this: *Nanoscale*, 2024, **16**, 635

A NIR-driven green affording-oxygen microrobot for targeted photodynamic therapy of tumors†

Lishan Zhang,‡[a] Xiaoting Zhang,‡[a] Hui Ran,‡[a] Ze Chen,[d] Yicheng Ye,[a] Jiamiao Jiang,[a] Ziwei Hu,[a] Miral Azechi,[a] Fei Peng,[c] Hao Tian,*[a] Zhili Xu*[b] and Yingfeng Tu*[a]

Photodynamic therapy (PDT) is a light-activated local treatment modality that has promising potential in cancer therapy. However, ineffective delivery of photosensitizers and hypoxia in the tumor microenvironment severely restrict the therapeutic efficacy of PDT. Herein, phototactic Chlorella (C) is utilized to carry photosensitizer-encapsulated nanoparticles to develop a near-infrared (NIR) driven green affording-oxygen microrobot system (CurNPs-C) for enhanced PDT. Photosensitizer (curcumin, Cur) loaded nanoparticles are first synthesized and then covalently attached to C through amide bonds. An *in vitro* study demonstrates that the developed CurNPs-C exhibits continuous oxygen generation and desirable phototaxis under NIR treatment. After intravenous injection, the initial 660 nm laser irradiation successfully induces the active migration of CurNPs-C to tumor sites for higher accumulation. Upon the second 660 nm laser treatment, CurNPs-C produces abundant oxygen, which in turn induces the natural product Cur to generate more reactive oxygen species (ROS) that significantly inhibit the growth of tumors in 4T1 tumor-bearing mice. This contribution showcases the ability of a light-driven green affording-oxygen microrobot to exhibit targeting capacity and O_2 generation for enhancing photodynamic therapy.

Received 31st July 2023,
Accepted 20th November 2023

DOI: 10.1039/d3nr03801g

rsc.li/nanoscale

Introduction

Cancer is one of the leading causes of death worldwide, while breast cancer is the most commonly diagnosed cancer in women and also the leading cause of premature death among women. Triple-negative breast cancer (TNBC), a heterogeneous subtype of breast cancer that lacks estrogen receptor, progesterone receptor, and human epidermal growth factor receptor 2, is the most aggressive cancer with few treatment options.[1–3] The current limitations of conventional cancer treatment include insufficient efficacy for tumor destruction and severe damage to normal tissues due to low selectivity. For instance, surgery often fails to completely eradicate the tumor.[4,5] Chemotherapy and radiotherapy are always accompanied by severe drug resistance and severe side effects, which have a negative impact on patients' quality of life.[6–8] Photodynamic therapy (PDT) is a promising light-based antitumor approach because it is less invasive than surgery, has no resistance compared to chemotherapy, and produces few side effects.[9,10] For PDT, there are three essential conditions including light, photosensitizers (PSs), and tissue oxygen. Normally, PSs in cancer cells or tumor tissues can be excited by light with a specific wavelength, resulting in the production of ROS with the involvement of oxygen. The resultant ROS can induce oxidative stress in cellular biomolecules, thus inducing cell death.[11–13] However, low supply of oxygen and poor delivery of photosensitizers in the tumor severely limit the efficacy of PDT.[14–16]

The hypoxia in a solid tumor is derived from the abnormal tumor vascular system and rapid tumor cell proliferation.[17,18] Since the hypoxic microenvironment significantly diminishes the therapeutic efficacy of PDT, numerous approaches have been used to improve the level of oxygen in tumors. These techniques can be divided into oxygen-carrying and oxygen-generating strategies. Oxygen-carrying strategies use the natural affinity of oxygen-binding materials (*e.g.*, fluorocarbon, hemoglobin) to supply exogenous O_2 to tumor tissue, while

[a]*Guangdong Provincial Key Laboratory of New Drug Screening, School of Pharmaceutical Sciences, Southern Medical University, Guangzhou 510515, China. E-mail: tianhao5588@126.com, tuyingfeng1@smu.edu.cn*
[b]*Department of Ultrasound, Institute of Ultrasound in Musculoskeletal Sports Medicine, Guangdong Second Provincial General Hospital, Guangzhou 510317, China. E-mail: zhili.xu@outlook.com*
[c]*School of Materials Science and Engineering, Sun Yat-Sen University, Guangzhou 510275, China*
[d]*Guangdong Key Laboratory of Nanomedicine, CAS-HK Joint Lab of Biomaterials, Shenzhen Engineering Laboratory of Nanomedicine and Nanoformulations, Institute of Biomedicine and Biotechnology, Shenzhen Institute of Advanced Technology (SIAT), Chinese Academy of Sciences, Shenzhen 518055, China*
†Electronic supplementary information (ESI) available. See DOI: **https://doi.org/10.1039/d3nr03801g**
‡These authors contributed equally to this work.

oxygen-generating strategies produce sufficient O_2 by *in situ* reactions (*e.g.*, photosynthesis, catalase catalysis) in tumors.[17,19] Compared to delivering O_2 through a carrier, *in situ* O_2 generation seems to be a more reasonable strategy because of the limited oxygen-loading capacity and rapid cargo leakage.[20] Photosynthesis, which is capable of highly efficient photocatalyzed O_2 generation, is a common photochemical reaction in nature; consequently, *in situ* O_2 generation *via* photosynthesis has also garnered considerable interest in the field of cancer therapy.[21–23] Chlorella is the earliest photosynthetic system on Earth, and its capacity to produce oxygen is dozens of times greater than that of common green plants. Due to its unique properties, Chlorella has been adopted as a bioengineering material to investigate the PDT-assisted effect.[24–26] For efficiently generating a high level of oxygen *in vitro* and *in vivo*, 660 nm near-infrared (NIR) light with better penetrating power is regarded as a viable candidate for biological application because of its favorable effect on Chlorella's photosynthesis.[25,27,28] On the cutting edge of cancer research, living system (including bacteria, algae, sperm, *etc.*)-based micro/nanorobots have been demonstrated with self-propulsion by utilizing the natural properties of living systems, which show considerable application potential in tumor-targeted therapy.[29–31] According to reports, Chlorella exhibits phototaxis that makes it move towards light, which could be used to construct a microrobot that delivers drugs to a specific site.[32] Therefore, Chlorella can not only relieve the hypoxia of tumors, but also act as a microrobot to effectively improve the delivery of photosensitizers, which simultaneously solves the two major issues in PDT. Curcumin, a polyphenol derived from the spice turmeric, is a natural photosensitizer that has remarkable safety and anticancer properties.[33,34] Curcumin also has the same problems as other photosensitizers, such as poor solubility and insufficient delivery.[35–37] By integrating curcumin into Chlorella through nanotechnology, the advantages of Chlorella can be effectively utilized to maximize the photodynamic therapeutic effect of curcumin.

Here, Chlorella (C) was modified with curcumin (Cur)-loaded human serum albumin (HSA) nanoparticles (CurNPs) to develop a NIR-driven green affording-oxygen microrobot (CurNPs-C) for boosted PDT therapy (Fig. 1). CurNPs were synthesized by a single-step sonication approach, followed by the activation of carboxy by EDC/NHS. Through the formation of amide bonds, CurNPs were covalently attached to the surface of C for the successful development of an engineering microrobot system. Our studies demonstrated that CurNPs-C maintained the photodynamic properties of CurNPs and the photosynthetic properties and the light chemotaxis of C. After intravenous injection, CurNPs-C exhibited good phototaxis and moved towards tumor tissue under initial 660 nm laser irradiation, resulting in a significant tumor accumulation of C and Cur. The second 660 nm laser irradiation was subsequently performed to promote the photosynthesis of enriched C for producing abundant O_2 in tumor tissue. Meanwhile, Cur gave full play to the role of PSs and produced sufficient ROS under the supply of oxygen, which finally induced cancer cell apoptosis and inhibited tumor growth effectively. Based on the natural properties of C, this biomimetic microrobot incorporated oxygen production and drug delivery capabilities for enhancing PDT, providing a momentous breakthrough for microbial-based tumor therapy.

Results and discussion

Preparation and characterization of CurNPs-C

The fabrication process of CurNPs-C is shown in Fig. 1A. First, CurNPs were obtained by assembling HSA and Cur under sonication. Then, the shape and size of the CurNPs were measured by transmission electron microscopy (TEM) and dynamic light scattering (DLS). As presented in Fig. S1 and S2,† CurNPs were uniformly spherical with a hydrodynamic size of 124.43 ± 1.33 nm. The carboxyl groups of CurNPs were activated with 1-(3-dimethylaminopropyl)-3-ethylcarbodiimide hydrochloride/*N*-hydroxysuccinimide (EDC/NHS), and the amine groups of C were then reacted with the activated carboxyl groups of CurNPs for the formation of CurNPs-C. Scanning electron microscopy (SEM) images demonstrated that CurNPs were successfully attached to the surface of C, and CurNPs-C remained spherical (Fig. 2A). The intense fluorescence (FL) signal of Cur on CurNPs-C can be observed in fluorescence microscopy images (Fig. 2B). Meanwhile, the UV–vis spectrum of CurNPs-C exhibited a characteristic absorption peak of C at 660 nm, and stronger absorption peaks were also observed at 280 nm and 436 nm (Fig. 2C). These results further indicated the successful attachment of CurNPs to C. Moreover, the FL emission spectra of CurNPs-C were also investigated. At the excitation wavelength of 436 nm, CurNPs-C showed fluorescence emission peaks at 547 nm and 673 nm, respectively (Fig. 2D). The results showed that CurNPs-C contained the fluorescence emission peak of CurNPs at 547 nm and the fluorescence emission peak of C at 673 nm, which further confirmed the successful attachment of CurNPs to C. The results also indicated that the FL properties of CurNPs-C are of great significance for *in vivo* imaging.

Next, we investigated the oxygen production of CurNPs-C under 660 nm laser irradiation. As shown in Fig. 2E and Table S1,† BG11 medium under 660 nm laser irradiation (control + NIR) and C in the dark would not produce oxygen, while C produced a large amount of oxygen under 660 nm laser irradiation. The result indicated that C possessed the ability to conduct photosynthetic oxygen production under 660 nm laser irradiation, which was beneficial for the PDT effect of hypoxic tumors. Meanwhile, the oxygen production of CurNPs and CurNPs-C under 660 nm laser irradiation was analyzed. The result demonstrated that the CurNPs would not produce oxygen in the presence or absence of 660 nm laser irradiation. Interestingly, the amount of oxygen produced by CurNPs-C under 660 nm laser irradiation was higher than that in the dark, and under the same conditions, the oxygen production of CurNPs-C was similar to that of C. The result showed that the introduction of CurNPs did not affect the

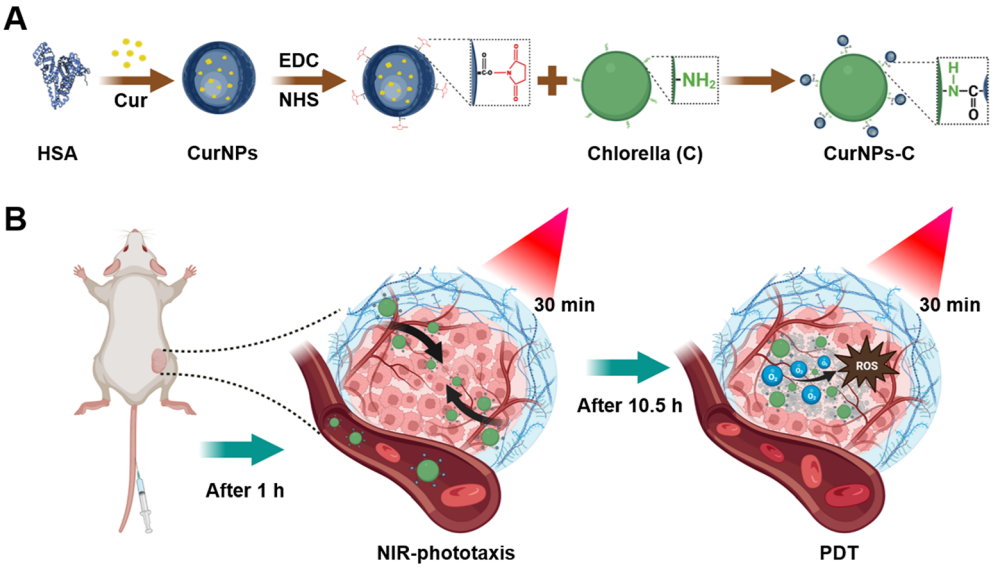

Fig. 1 The design and function of a NIR-driven green affording-oxygen microrobot (CurNPs-C) for tumor treatment. (A) CurNPs were produced by a single-step sonication approach, and the carboxyl groups of CurNPs were activated using EDC/NHS. Carboxyl-activated CurNPs were attached to C through amide bonds to form CurNPs-C. (B) NIR-driven CurNPs-C moved towards tumor tissue under initial 660 nm laser irradiation, resulting in a significant accumulation of C and CurNPs in the tumor. Under the second laser irradiation, CurNPs-C produced abundant O_2 in the tumor, and Cur generated a large amount of ROS through a PDT reaction, effectively inducing the apoptosis of cancer cells and inhibiting tumor growth. Note: HSA: human serum albumin; Cur: curcumin; CurNPs: Cur loaded HSA nanoparticles; EDC: 1-(3-dimethylaminopropyl)-3-ethylcarbodiimide hydrochloride; NHS: *N*-hydroxysuccinimide; C: Chlorella; CurNPs-C: CurNPs attached C; NIR: near-infrared; PDT: photodynamic therapy.

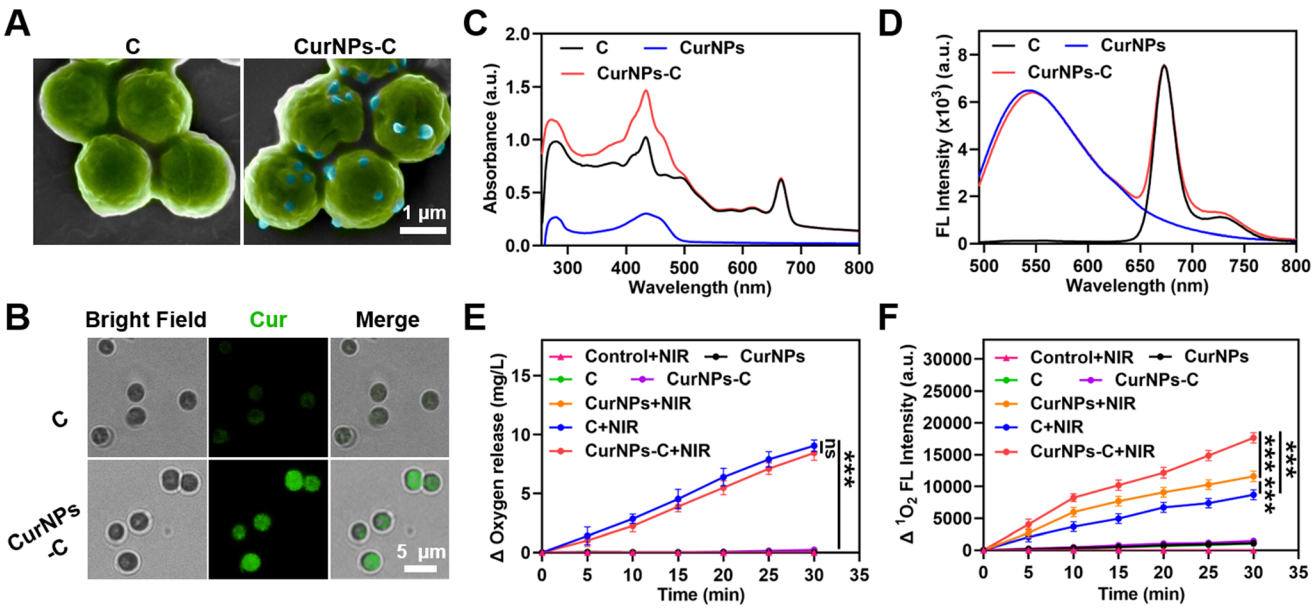

Fig. 2 The characteristics of CurNPs-C. (A) SEM images of C and CurNPs-C, demonstrating the attachment of CurNPs to C. (B) FL images of C and CurNPs-C. (C) The UV-Vis-NIR absorption spectra of C, CurNPs, and CurNPs-C in DMSO solution. (D) The FL spectra of C, CurNPs, and CurNPs-C in DMSO solution. (E) Oxygen production curves of the control + NIR, C, CurNPs, and CurNPs-C groups treated without or with 660 nm laser irradiation (0.1 W cm^{-2}) (n = 3). (F) $^1O_2$ generation curves of the control + NIR, C, CurNPs, and CurNPs-C groups treated without or with 660 nm laser irradiation (0.1 W cm^{-2}) (n = 3). Statistical analysis was conducted by one-way ANOVA analysis followed by Tukey's post-test (*p < 0.05, **p < 0.01, ***p < 0.001). ns indicates no significant difference.

oxygen production of C under 660 nm laser irradiation, which was crucial for the PDT effect of photosensitizers. To estimate the PDT effect of CurNPs-C, the production of singlet oxygen ($^1O_2$) in BG11 medium was measured using singlet oxygen sensor green (SOSG) under 660 nm laser irradiation. As shown in Fig. 2F, BG11 medium under 660 nm laser irradiation

(control + NIR) and C, CurNPs or CurNPs-C in the dark would not produce $^1O_2$. However, CurNPs produced more $^1O_2$ than C under 660 nm laser irradiation and CurNPs-C significantly enhanced the production of $^1O_2$ under 660 nm laser irradiation, indicating that the PDT effect of CurNPs-C was greatly improved (Fig. 2F and Table S2†). The result proved that CurNPs-C could relieve hypoxia in tumors, generate abundant ROS to induce tumor cell death and inhibit tumor growth through oxidative stress, and thus possess huge potential for application in PDT.

NIR-phototaxis behavior and PDT efficiency in 4T1 cells

To test the light-driven migration ability, C or CurNPs-C solutions were cultured on a foil-wrapped culture dish, where one corner of the culture dish was exposed to a light source, and the movement of C or CurNPs-C with time under the influence of the light source was observed (Fig. 3A).

First, we investigated the light-driven migration ability of C or CurNPs-C solutions under the influence of white light. As shown in Fig. S3,† C or CurNPs-C moved towards the side exposed to white light, indicating their light-driven migration ability and proving that the presence of CurNPs did not affect the light-chemotaxis ability of C. Next, we studied the NIR-driven migration ability of C or CurNPs-C solutions under the influence of 660 nm laser irradiation. As shown in Fig. 3B, C or CurNPs-C moved towards the side illuminated by 660 nm laser irradiation after 30 min of treatment. As time passed, C or CurNPs-C was enriched more, and a clear green spot was generated near the NIR light source after 1 h of illumination. Therefore, the experiment of lateral exposure to NIR light confirmed the NIR-driven migration ability of CurNPs-C, which provided an important basis for the enrichment of CurNPs-C through *in vivo* illumination.

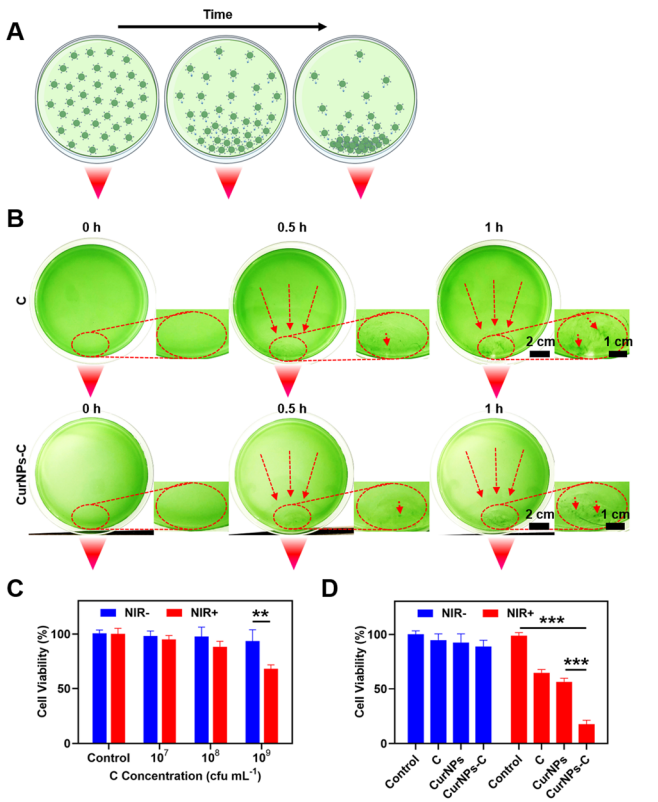

Fig. 3 *In vitro* NIR-driven migration behavior and PDT efficiency of CurNPs-C. (A) Schematic illustration of the NIR-driven experiment design. CurNPs-C was inoculated in a Petri dish under 660 nm laser irradiation on one side (0.1 W cm^{-2}). (B) Photographs of the NIR-driven experiment of CurNPs-C in the Petri dish under 660 nm laser irradiation on one side (0.1 W cm^{-2}). (C) The biosafety of C at different concentrations to 4T1 cells (8 × 10^3 cells per well) (n = 3). (D) The phototoxicity of CurNPs-C to 4T1 cells (8 × 10^3 cells per well) without or with 660 nm laser irradiation (0.1 W cm^{-2}) (n = 3). Statistical analysis was conducted by one-way ANOVA analysis followed by Tukey's post-test (*p < 0.05, **p < 0.01, ***p < 0.001). ns indicates no significant difference.

We further tested the biocompatibility and PDT-mediated cell death of CurNPs-C *in vitro*. First, the biosafety of C to 4T1 cells was determined using the cell counting kit-8 (CCK-8) assay in the absence of light. The results showed that C did not cause obvious toxicity to 4T1 cells at a concentration below 10^9 cfu per mL without light treatment (Fig. 3C and Table S3†). Furthermore, the PDT-mediated tumor killing effect of C on 4T1 cells was investigated under 660 nm laser irradiation. As revealed in Fig. 3C, the cytotoxicity was relatively low in the groups with C concentrations of 10^7 cfu per mL and 10^8 cfu per mL under 660 nm laser irradiation, while obvious cytotoxicity occurred in the group with a C concentration of 10^9 cfu per mL treated with 660 nm laser irradiation. We chose a C concentration of 10^9 cfu per mL for the subsequent 4T1 tumor-killing experiment. Next, we tested the PDT-mediated tumor killing ability of C, CurNPs, and CurNPs-C. As revealed in Fig. 3D and Table S4,† the 4T1 cells in the C, CurNPs, and CurNPs-C groups did not show significant cytotoxicity under dark conditions. However, approximately 35% of 4T1 cells died in the C + NIR group and approximately 43% of 4T1 cells underwent apoptosis in the CurNPs + NIR group, while over 80% of 4T1 cells did not survive in the CurNPs-C + NIR group, indicating that CurNPs-C had an effective PDT effect on 4T1 cancer cells under 660 nm laser irradiation.

Biodistribution of CurNPs-C

To determine whether the accumulation of C in tumors could be increased under 660 nm laser irradiation, 4T1 tumor-bearing mice were randomly divided into two groups: the C group and the C + NIR group. These mice were intravenously (i.v.) injected with C, and the tumor of the C + NIR group was subjected to sequential irradiation with a 660 nm laser for 30 min at 1 h after intravenous injection. Subsequently, tumors from 4T1 tumor-bearing mice at 6 h or 12 h post administration were collected, ground and further coated on solid BG11 agar culture medium. After incubation for 48 h, the quantity of C in tumor tissue was quantified by colony counting. The results showed that the number of C colonies (normalized by weight; cfu per g) of the C + NIR group was much higher than that of the C group at 6 h or 12 h after intravenous injection (Fig. S4 and Table S5†). The results demonstrated that 660 nm laser irradiation could significantly increase the

accumulation of C in tumors, indicating the effectiveness of C phototaxis *in vivo*.

Also, in order to determine whether the accumulation of NIR-driven CurNPs-C in tumors can be increased under 660 nm laser irradiation, 4T1 tumor-bearing mice were randomly divided into three groups: the CurNPs group, the CurNPs-C group, and the CurNPs-C + NIR group. These mice were intravenously (i.v.) injected with CurNPs or CurNPs-C, and the tumor of the CurNPs-C + NIR group was subjected to sequential irradiation with a 660 nm laser for 30 min at 1 h after intravenous injection. Subsequently, tumors from 4T1 tumor-bearing mice at 6 h or 12 h after intravenous injection were collected, ground and further coated on solid BG11 agar culture medium for incubation. After incubation for 48 h, the quantity of C in tumor tissue was quantified by colony counting. The results showed that there were no C colonies in the CurNPs group, and the number of C colonies (normalized by weight; cfu per g) of the CurNPs-C group was similar to that of the C group, and that of the CurNPs-C + NIR group was comparable to that of the C + NIR group (Fig. S4,† Fig. 4A, B, Tables S5 and S6†). And 12 h after intravenous injection, the number of C colonies in the CurNPs-C + NIR group was more than 1.75 times higher than that of the CurNPs-C group. The results demonstrated that 660 nm laser irradiation of tumors from 4T1 tumor-bearing mice can increase the accumulation of CurNPs-C in tumors.

To explore the tumor targeting delivery effect of C and Cur in the CurNPs-C + NIR group, the 4T1 tumor-bearing mice were injected with CurNPs or CurNPs-C intravenously, and the tumor of the CurNPs-C + NIR group was subjected to sequential irradiation with a 660 nm laser for 30 min at 1 h after intravenous injection. The 4T1 tumor-bearing mice were sacrificed 12 h after the intravenous injection and the main organs and tumors were collected to measure the FL signals of Cur with the *in vivo* imaging system (IVIS). *In vivo* imaging results showed that there was no fluorescence of C in the CurNPs group, and C was the most abundant in tumors in the CurNPs-C + NIR group (Fig. 4C, D and Table S7†). Also, Cur was the least abundant in tumors in the CurNPs group, and Cur was the most abundant in tumors in the CurNPs-C + NIR group, which confirmed that NIR-driven CurNPs-C enhanced the tumor-targeted drug delivery in 4T1 tumor-bearing mice under 660 nm laser irradiation (Fig. 4E, F and Table S8†).

The accumulation and infiltration of Cur in the tumor were further analysed using immunofluorescence imaging. The tissue immunofluorescence showed that Cur was mainly distributed in blood vessels in the CurNPs group, and the highest Cur infiltration was observed in the CurNPs-C + NIR group (Fig. 4G).

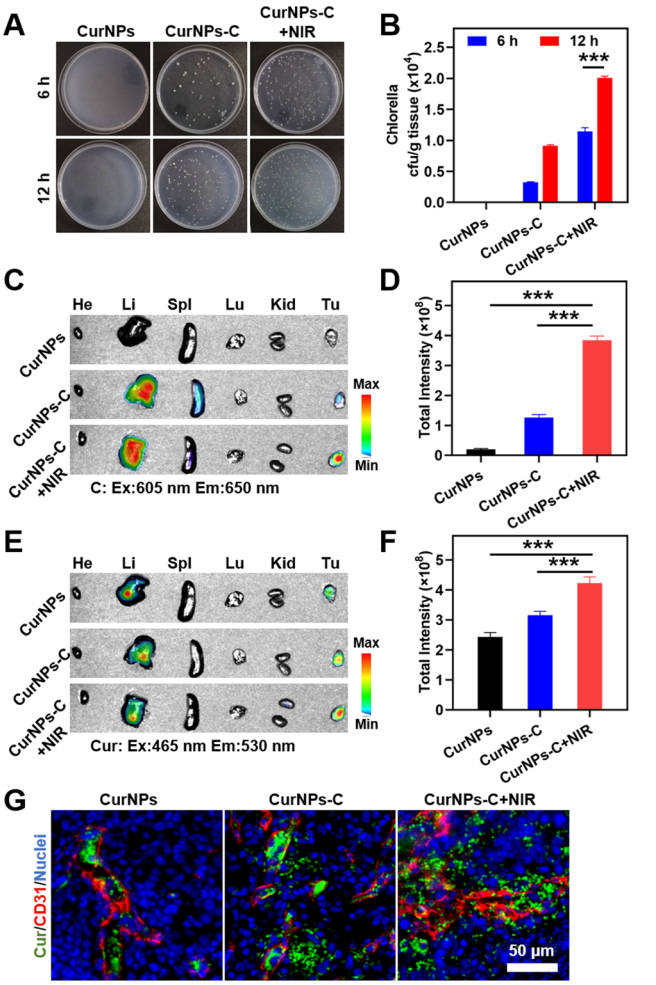

Fig. 4 *In vivo* biodistribution of CurNPs-C. Plate coating image photographs (A) and colony numbers (B) of tumor tissue homogenates from 4T1 tumor-bearing mice in the CurNPs, CurNPs-C, and CurNPs + NIR groups at different times after intravenous injection (n = 3). (C) *Ex vivo* fluorescence images of C of the major organs and tumors of 4T1 tumor-bearing mice in the CurNPs, CurNPs-C, and CurNPs + NIR groups 12 h after intravenous injection. (D) The semi-quantification of the total fluorescence intensity for the accumulation of C in the tumor of each group (n = 3). (E) *Ex vivo* fluorescence images of Cur of the major organs and tumors of 4T1 tumor-bearing mice in the CurNPs, CurNPs-C, and CurNPs + NIR groups 12 h after intravenous injection. (F) The semi-quantification of the total fluorescence intensity for the accumulation of Cur in the tumor of each group (n = 3). (G) Histological section of the tumors stained with anti-CD31 antibodies (blood vessels, red) of 4T1 tumor-bearing mice in the CurNPs, CurNPs-C, and CurNPs + NIR groups 12 h after intravenous injection (Cur, green). Statistical analysis was conducted by one-way ANOVA analysis followed by Tukey's post-test (*p < 0.05, **p < 0.01, ***p < 0.001). ns indicates no significant difference. Note: He: heart; Li: liver; Spl: spleen; Lu: lungs; Kid: kidneys; Tu: tumor.

Antitumor effect of CurNPs-C

To investigate the PDT efficiency of CurNPs-C, 4T tumor-bearing mice were randomly divided into five groups: the PBS + NIR group, the C + NIR group, the CurNPs + NIR group, the CurNPs-C group, and the CurNPs-C + NIR group. The experimental plan is shown in Fig. 5A. Briefly, 4T1 tumor-bearing mice were injected with PBS, C, CurNPs, or CurNPs-C intravenously (i.v.) on days 1, 3, 5, and 7, respectively. And the tumors in the PBS + NIR group, the C + NIR group, the CurNPs + NIR group, and the CurNPs-C + NIR group were irradiated

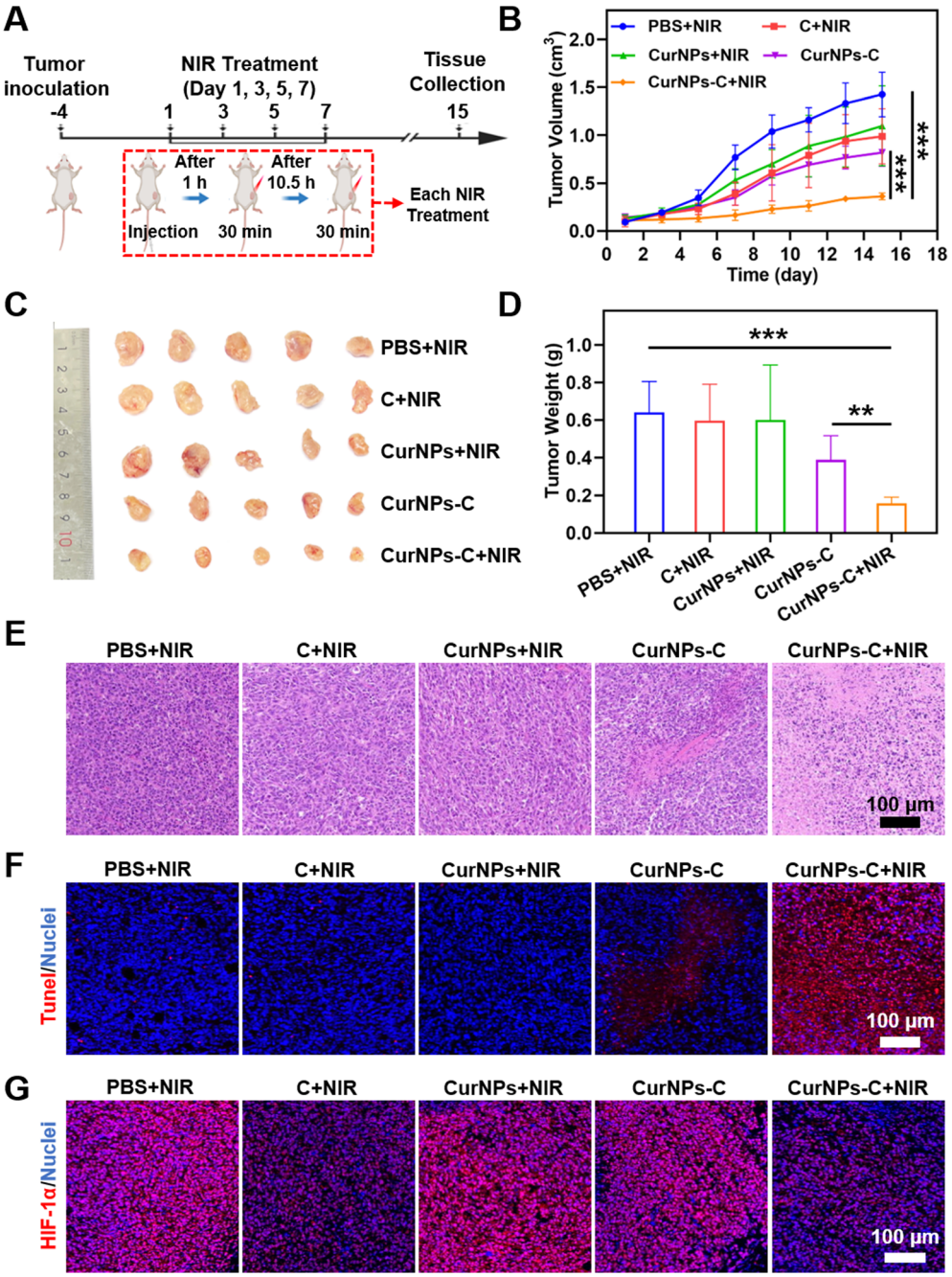

Fig. 5 *In vivo* PDT-mediated antitumor effect of CurNPs-C. (A) The therapeutic protocol in 4T1 tumor-bearing mice for evaluating the antitumor effect of PDT. Different treatments were repeated on days 1, 3, 5, and 7. (B) The tumor volume evolution of 4T1 tumor-bearing mice during different treatments (n = 5). (C) The photos of tumors after different treatments. (D) The tumor weight of tumors after different treatments (n = 5). (E–G) Micrographs of histological sections of tumors stained with hematoxylin and eosin (H&E) (E), TdT-mediated dUTP nick-end labeling (TUNEL) (F) and HIF-1α (G) after different treatments. Statistical analysis was conducted by Student's t-tests (*p < 0.05, **p < 0.01, ***p < 0.001). ns indicates no significant difference.

with a 660 nm laser for 30 min at 1 h and 12 h after intravenous injection. During the treatment period, we determined the treatment efficiency by recording the tumor volume of each group (Fig. 5B and Table S9†). The results showed that the tumor grew rapidly in the PBS + NIR group, indicating that the impact of 660 nm laser irradiation therapy alone on tumor inhibition can be negligible. In addition, the C + NIR and CurNPs + NIR groups had an inhibitory effect on the growth with an unsatisfactory antitumor effect. Also, CurNPs-C can inhibit tumor growth, which may be due to the increased accumulation of Cur in tumors by C. Interestingly, the CurNPs-C + NIR group showed significant tumor suppression,

indicating that CurNPs-C + NIR has a strong PDT-mediated anti-tumor effect. At the end of the treatment, 4T1 tumor-bearing mice were sacrificed, and tumor tissue was collected for observation. As presented in Fig. 5C, the CurNPs C + NIR group had the smallest tumor among all groups, indicating that CurNPs-C possessed the best treatment effect under 660 nm laser irradiation. In addition, we weighed and recorded the tumors after treatment. As shown in Fig. 5D and Table S10,† the CurNPs-C + NIR group had the lightest tumor weight, further demonstrating the PDT treatment effect of CurNPs-C under 660 nm laser irradiation. Finally, microscopic evaluation of tumor sections was carried out by H&E staining and TdT-mediated dUTP nick-end labeling (TUNEL) assay. As shown in Fig. 5E and F, Fig. S5 and Table S11,† there was no evident variation of the cell state in the PBS + NIR group, while minor destruction was observed in the C + NIR, CurNPs + NIR, and CurNPs-C groups. However, a large amount of tumor cells induced damage or apoptosis in the CurNPs-C + NIR group, which confirmed the anti-tumor effect of CurNPs-C under 660 nm laser irradiation. The tumor sections were stained with HIF-1α to determine whether the tumor hypoxia could be ameliorated by the photosynthesis of C *in vivo*. As shown in Fig. 5G, the group treated with PBS + NIR displayed a strong red fluorescence signal because of the presence of extensive areas of hypoxia. Moreover, the hypoxia areas were aggravated in the CurNPs + NIR group, indicating that the oxygen was consumed by PDT. In contrast, hypoxia was alleviated in the C + NIR and CurNPs-C + NIR groups.

We studied the biodegradability of CurNPs-C. 4T1 tumor-bearing mice were injected with CurNPs-C intravenously (i.v.) with a 660 nm laser for 30 min at 1 h and 12 h after intravenous injection. Tumors and kidneys were collected and ground on days 1, 3, 7, 15, and 18 and further coated on solid BG11 agar culture medium for incubation. After incubation for 48 h, the quantity of C in tumor tissue was quantified by colony counting (normalized by weight; cfu per g). As shown in Fig. S6,† the number of C colonies (normalized by weight; cfu per g) decreased over time. No C colonies were detected in the kidneys on day 15, and no C colonies were detected in tumors on day 18, indicating the clearance of CurNPs-C.

We also studied the biosafety of CurNPs-C. As shown in Fig. S7†, there was no significant change in the body weight of each group during the treatment period, indicating that 660 nm laser irradiation and CurNPs-C had good biosafety. In addition, serum liver indicators (ALT/AST) and serum renal indicators (UREA/CREA-S) were evaluated at the end of treatment to assess the hepatorenal toxicity of CurNPs-C (Fig. S8†). There were no significant differences between each group, indicating the biosafety of 660 nm laser irradiation and CurNPs-C. In addition, the biological safety of the main organs of mice was further evaluated by H&E staining (Fig. S9†). Heart, liver, spleen, lung, and kidney tissue sections stained with H&E revealed no obvious lesions in various groups. These results further confirmed the biosafety of 660 nm laser irradiation and CurNPs-C.

Conclusions

In conclusion, we constructed a novel light-driven green affording-oxygen microrobot through a single-step sonication approach and an amidation reaction that has a robust PDT therapeutic effect in the treatment of triple-negative breast cancer. After injecting biomimetic CurNPs-C, successive chemotactic enrichment was achieved upon the first NIR laser irradiation. With the second laser treatment, CurNPs-C produced abundant oxygen in tumor tissue and further generated more ROS to kill cancer cells and exhibited robust tumor inhibition. This Chlorella-based biosystem provides new insight for developing PDT models with active chemotaxis and efficient microenvironment adjustment, which expands the application of microorganisms in the biomedical field, particularly for enhancing the PDT effect in tumor treatment.

Experimental

Materials and reagents

N-Hydroxysuccinimide (NHS), 1-(3-dimethylaminopropyl)-3-ethylcarbodiimide hydrochloride (EDC), and 2-(*N*-morpholino)-ethane sulfonic acid (MES) were all acquired from Aladdin (China). Curcumin was acquired from Sigma-Aldrich (USA). Singlet oxygen sensor green (SOSG) was acquired from Invitrogen (USA). 4T1 murine breast tumor cells were purchased from the Cell Bank of Type Culture Collection of the Chinese Academy of Sciences (China). Chlorella and BG11 medium were derived from the freshwater algae seed bank at the Institute of Hydrobiology (China). All animal procedures were performed in accordance with the Guidelines for the Institutional Animal Care and Use Committee (IACUC) and approved by the Animal Ethics Committee of Southern Medical University.

Preparation and characterization of CurNPs and CurNPs-C

CurNPs were formed by dropping 200 μL of Cur solution (2.5 mg mL^{-1}, dimethyl sulfoxide solvent) into 4 mL of HSA solution (2.5 mg mL^{-1}, pure water) under sonication.[38] Then EDC and sulfo-NHS were dissolved in 12 mL of MES buffer solution and mixed with CurNPs at 25 °C for 1 h to form active CurNPs. Then they were dialyzed with H_2O to obtain a mixture. To form CurNPs-C, C and activated CurNPs were mixed for 1 h at 25 °C. Finally, the mixture was centrifuged to remove unbound CurNPs, washed with PBS three times, and then CurNPs-C was collected.

Scanning electron micrographs (SEM, Quattro S, Thermo, USA), transmission electron micrographs (TEM, JEOL-1400, Japan), and a fluorescence microscope (Eclipse Ti2, Nikon, Japan) were used to identify the morphology of CurNPs, C, and CurNPs-C. The absorption spectrum was recorded using a UV-vis spectrometer (Shimadzu UV-2600, Japan) and the fluorescence spectrum was recorded using a fluorescence spectrophotometer (Shimadzu RF-6000, Japan). The hydrodynamic

diameters of CurNPs were measured by dynamic light scattering (DLS, Malvern Zetasizer Nano ZSE, UK).

In vitro oxygen production by photosynthesis

CurNPs, C, or CurNPs-C (10 μg mL^{-1} of Cur, 1×10^9 cfu per mL of C in 10 mL BG11 medium) were exposed to 660 nm laser irradiation (0.1 W cm^{-2}, 30 min) or darkness, and oxygen production was measured using a dissolved oxygen meter (JPBJ-609L, China). The probe was injected into the CurNPs, C, or CurNPs-C solution and the value of dissolved oxygen was recorded at the specified time.

In vitro singlet oxygen detection

According to the manufacturer's protocol, singlet oxygen sensor green (SOSG, Invitrogen) was used to detect *in vitro* singlet oxygen produced by CurNPs, C, or CurNPs-C in BG11 medium under 660 nm laser irradiation (0.1 W cm^{-2}, 30 min) or in the dark.

NIR-driven migration ability of CurNPs-C

To test the NIR-driven migration ability of CurNPs-C, BG11 medium was poured into a Petri dish and 10^9 cfu per mL containing C or CurNPs-C were inoculated on BG11 medium. The Petri dish was wrapped in tin foil and exposed to white light or 660 nm laser irradiation from one side (0.1 W cm^{-2}, 1 h). Meanwhile, the migration of C or CurNPs-C was monitored.

Evaluation of *in vitro* biosafety and PDT efficacy

4T1 tumor cells (8×10^3 cells per well) were incubated in 96-well plates and cultured for 12 h. Then the culture medium was replaced with C solution (C concentrations of 10^7, 10^8, and 10^9 cfu per mL), incubated for 3 hours, and then 4T1 tumor cells were treated with 660 nm laser irradiation (0.1 W cm^{-2}) or kept in the dark. After 24 hours of incubation, the cell survival rate was measured using the cell counting kit-8 (CCK-8) assay.

To study the anti-tumor effect of PDT of CurNPs-C, 4T1 tumor cells (8×10^3 cells per well) were incubated in 96-well plates and cultured for 12 h. Then the culture medium was replaced with C, CurNPs, or CurNPs-C solution (C concentration of 10^9 cfu per mL), incubated for 3 hours, and then the 4T1 tumor cells were treated with 660 nm laser irradiation (0.1 W cm^{-2}, 30 min) or kept in the dark. After 24 hours of incubation, the cell survival rate was measured using the cell counting kit-8 (CCK-8) assay.

Chlorella colonization and FL imaging

4T1 tumor-bearing mice (six weeks old female Balb/c mice) were randomly divided into two groups (n = 3): the C group the and C + NIR group (the concentration of C was 10^9 cfu per mL). When the tumor volume reached about 600 mm^3, 4T1 tumor-bearing mice were intravenously (i.v.) injected with C, and the tumor of the C + NIR group was subjected to sequential irradiation with a 660 nm laser irradiation (0.1 W cm^{-2}) for 30 min at 1 h after injection. We collected tumors from 4T1 tumor-bearing mice 6 h or 12 h after intravenous injection. The tumors were extracted, weighed, and homogenized in sterile PBS (pH = 7.2). These samples were diluted (10 times) and plated on BG11 medium. After 6 h of incubation, the colonies of tumor tissues in each group were counted. Bacterial titer (CFU per gram of tissue) was calculated using colony count and tissue weight.

4T1 tumor-bearing mice (six weeks old female Balb/c mice) were randomly divided into three groups (n = 3): the CurNPs group, the CurNPs-C group, and the CurNPs-C + NIR group (the concentration of C was 10^9 cfu per mL, and the concentration of Cur was 10 μg mL^{-1}). When the tumor volume reached about 600 mm^3, 4T1 tumor-bearing mice were intravenously (i.v.) injected with CurNPs or CurNPs-C, and the tumor of the CurNPs-C + NIR group was subjected to sequential irradiation with a 660 nm laser(0.1 W cm^{-2}) for 30 min at 1 h after intravenous injection. We collected tumors from 4T1 tumor-bearing mice 6 h or 12 h after intravenous injection. The tumors were extracted, weighed, and homogenized in sterile PBS (pH = 7.2). These samples were diluted (10 times) and plated on BG11 medium. After 6 h of incubation, the colonies of tumor tissues in each group were counted. Bacterial titer (CFU per gram of tissue) was calculated using colony count and tissue weight.

4T1 tumor-bearing mice 12 h after intravenous injection of the above treatment were sacrificed with high concentration carbon dioxide, and the main organs, including the heart, liver, spleen, lungs, kidneys, and tumor were extracted. The *in vivo* imaging system (IVIS) was used to test the accumulation of C (Ex: 605 nm; Em: 650 nm) and Cur (Ex: 465 nm; Em: 530 nm) in the main organs and tumors. And the tumor sections stained with CD31 (blood vessels, red) were analyzed with a microscope.

In vivo PDT tumor treatment

4T1 tumor-bearing mice (six weeks old female Balb/c mice) were randomly divided into five groups (n = 5): the PBS + NIR, C + NIR, CurNPs + NIR, CurNPs-C, and CurNPs-C + NIR groups (the concentration of C was 10^9 cfu per mL, and the concentration of Cur was 10 μg mL^{-1}). When the tumor volume reached about 100 mm^3, 4T1 tumor-bearing mice were intravenously (i.v.) injected with CurNPs, C, or CurNPs-C on days 1, 3, 5, and 7, and the tumors of the PBS + NIR, C + NIR, CurNPs + NIR, and CurNPs-C + NIR groups were subjected to sequential irradiation with a 660 nm laser irradiation (0.1 W cm^{-2}) for 30 min at 1 h or 12 h after intravenous injection. To investigate the PDT-based antitumor effect, body weight and tumor volume were measured every other day ($V = (ab^2)/2$, where a and b are the length and width of the tumor, respectively). 15 days after tumor treatment, 4T1 tumor-bearing mice were euthanized and their tumors, main organs, and serum were taken. Photos were taken and the tumor weight of 4T1 tumor-bearing mice of each group was measured to study the PDT-mediated anti-tumor effect of CurNPs-C. And after slicing, H&E staining and the TdT-mediated dUTP nick-end labeling (TUNEL) assay of the tumor, the tumor inhibitory effect of

CurNPs-C was studied by observing cell apoptosis or necrosis. HIF-1α staining was conducted to detect the effect of the photosynthesis of C *in vivo* on tumor hypoxia.

To study biosafety, histological analysis was conducted on the main organs of 4T1 tumor-bearing mice 15 days after tumor treatment, and tissue sections stained with H&E were analyzed with a microscope. To assess the hepatorenal toxicity of CurNPs-C, liver indicators (ALT/AST) and serum renal indicators (UREA/CREA-S) were evaluated using a liver or renal function activity assay kit.

To study the biodegradability of CurNPs-C, 4T1 tumor-bearing mice were intravenously (i.v.) injected with CurNPs-C, and the tumor was subjected to sequential irradiation with a 660 nm laser (0.1 W cm^{-2}) for 30 min at 1 h after intravenous injection. We collected tumors from 4T1 tumor-bearing mice on days 1, 3, 7, 15, and 18, and the number of C colonies was counted by tumor tissue coating.

Statistical analysis

Statistical analysis was conducted using Student's *t*-test or one-way ANOVA analysis followed by Tukey's post-test, and the experimental data were expressed as means ± SD. The asterisk denoted statistical significance: $*p < 0.05$, $**p < 0.01$, $***p < 0.001$.

Author contributions

The manuscript was written through the contributions of all authors. All authors have given approval to the final version of the manuscript.

Conflicts of interest

The authors declare no conflict of interest.

Acknowledgements

This work was supported by the National Key Research and Development Program of China (2022YFA1206900), the National Natural Science Foundation of China (no. 22175083, 51973241, and 82102051), and the Guangzhou Basic and Applied Basic Research Foundation (202201011078).

References

1 B. S. Chhikara and K. Parang, *Chem. Biol. Lett.*, 2023, **10**, 451–451.
2 Y. Liu, N. Qiu, L. Shen, Q. Liu, J. Zhang, Y.-Y. Cheng, K.-H. Lee and L. Huang, *J. Controlled Release*, 2020, **323**, 431–441.
3 F. Derakhshan and J. S. Reis-Filho, *Annu. Rev. Pathol.: Mech. Dis.*, 2022, **17**, 181–204.
4 J. C. Coffey, J. Wang, M. Smith, D. Bouchier-Hayes, T. Cotter and H. Redmond, *Lancet Oncol.*, 2003, **4**, 760–768.
5 L. Cheng, C. Wang, L. Feng, K. Yang and Z. Liu, *Chem. Rev.*, 2014, **114**, 10869–10939.
6 D. De Ruysscher, G. Niedermann, N. G. Burnet, S. Siva, A. W. Lee and F. Hegi-Johnson, *Nat. Rev. Dis. Primers*, 2019, **5**, 13.
7 J. L. Markman, A. Rekechenetskiy, E. Holler and J. Y. Ljubimova, *Adv. Drug Delivery Rev.*, 2013, **65**, 1866–1879.
8 Q. He and J. Shi, *Adv. Mater.*, 2014, **26**, 391–411.
9 K. Rhew, Y.-J. Chae and J.-E. Chang, *J. Pharm. Invest.*, 2022, **52**, 587–599.
10 S. S. Lucky, K. C. Soo and Y. Zhang, *Chem. Rev.*, 2015, **115**, 1990–2042.
11 J. Choi, I.-C. Sun, H. S. Hwang, H. Y. Yoon and K. Kim, *Adv. Drug Delivery Rev.*, 2022, **186**, 114344.
12 J. F. Algorri, M. Ochoa, P. Roldán-Varona, L. Rodríguez-Cobo and J. M. López-Higuera, *Cancers*, 2021, **13**, 4447.
13 S. Li, F. Yang, Y. Wang, T. Du and X. Hou, *Chem. Eng. J.*, 2023, **451**, 138621.
14 W. Tang, Z. Zhen, M. Wang, H. Wang, Y. J. Chuang, W. Zhang, G. D. Wang, T. Todd, T. Cowger and H. Chen, *Adv. Funct. Mater.*, 2016, **26**, 1757–1768.
15 X.-T. Yu, S.-Y. Sui, Y.-X. He, C.-H. Yu and Q. Peng, *Biomater. Adv.*, 2022, **135**, 212725.
16 G. Yang, J. Tian, C. Chen, D. Jiang, Y. Xue, C. Wang, Y. Gao and W. Zhang, *Chem. Sci.*, 2019, **10**, 5766–5772.
17 Q. Zhou, F. Mohammed, Y. Wang, J. Wang, N. Lu, J. Li and Z. Ge, *J. Controlled Release*, 2021, **339**, 130–142.
18 A. Emami Nejad, S. Najafgholian, A. Rostami, A. Sistani, S. Shojaeifar, M. Esparvarinha, R. Nedaeinia, S. Haghjooy Javanmard, M. Taherian and M. Ahmadlou, *Cancer Cell Int.*, 2021, **21**, 1–26.
19 J. Hu, Z. Guan and J. Chen, *Cancer Lett.*, 2021, **521**, 39–49.
20 Y. Wan, L. H. Fu, C. Li, J. Lin and P. Huang, *Adv. Mater.*, 2021, **33**, 2103978.
21 X. Li, L. Chen, M. Huang, S. Zeng, J. Zheng, S. Peng, Y. Wang, H. Cheng and S. Li, *Asian J. Pharm. Sci.*, 2023, **18**, 100775.
22 Y. Qiao, F. Yang, T. Xie, Z. Du, D. Zhong, Y. Qi, Y. Li, W. Li, Z. Lu and J. Rao, *Sci. Adv.*, 2020, **6**, eaba5996.
23 S. Qin, Y. Xu, H. Li, H. Chen and Z. Yuan, *Biomater. Sci.*, 2022, **10**, 51–84.
24 W. Li, D. Zhong, S. Hua, Z. Du and M. Zhou, *ACS Appl. Mater. Interfaces*, 2020, **12**, 44541–44553.
25 H. Wang, Y. Guo, C. Wang, X. Jiang, H. Liu, A. Yuan, J. Yan, Y. Hu and J. Wu, *Biomaterials*, 2021, **269**, 120621.
26 M. Ou, C. Lin, Y. Wang, Y. Lu, W. Wang, Z. Li, W. Zeng, X. Zeng, X. Ji and L. Mei, *J. Controlled Release*, 2022, **345**, 755–769.
27 C. Lee, K. Lim, S. S. Kim, E. S. Lee, K. T. Oh, H.-G. Choi and Y. S. Youn, *J. Controlled Release*, 2019, **294**, 77–90.
28 H. Wang, H. Liu, Y. Guo, W. Zai, X. Li, W. Xiong, X. Zhao, Y. Yao, Y. Hu and Z. Zou, *Bioact. Mater.*, 2022, **12**, 97–106.

29 W. Xu, H. Qin, H. Tian, L. Liu, J. Gao, F. Peng and Y. Tu, *Appl. Mater. Today*, 2022, **27**, 101482.
30 H. Li, F. Peng, X. Yan, C. Mao, X. Ma, D. A. Wilson, Q. He and Y. Tu, *Acta Pharm. Sin. B*, 2022, **13**, 517–541.
31 L. Liu, H. He, Z. Luo, H. Zhou, R. Liang, H. Pan, Y. Ma and L. Cai, *Adv. Funct. Mater.*, 2020, **30**, 1910176.
32 V. V. Zaitsev, V. V. Petryakov, L. M. Zaitseva and Z. N. Makhimova, *Samara J. Sci.*, 2022, **11**, 52–56.
33 M. Sun, Y. Zhang, Y. He, M. Xiong, H. Huang, S. Pei, J. Liao, Y. Wang and D. Shao, *Colloids Surf., B*, 2019, **180**, 313–318.
34 F. C. Machado, R. P. A. de Matos, F. L. Primo, A. C. Tedesco, P. Rahal and M. F. Calmon, *Bioorg. Med. Chem.*, 2019, **27**, 1882–1890.
35 A. Yuan, B. Yang, J. Wu, Y. Hu and X. Ming, *Acta Biomater.*, 2015, **21**, 63–73.
36 F. da Silva Feltrin, T. Agner, C. Sayer and L. M. F. Lona, *Adv. Colloid Interface Sci.*, 2022, **300**, 102582.
37 M. Cozzolino, P. Delcanale, C. Montali, M. Tognolini, C. Giorgio, M. Corrado, L. Cavanna, P. Bianchini, A. Diaspro and S. Abbruzzetti, *Life Sci.*, 2019, **233**, 116710.
38 A. Ma, H. Chen, Y. Cui, Z. Luo, R. Liang, Z. Wu, Z. Chen, T. Yin, J. Ni and M. Zheng, *Small*, 2019, **15**, 1804028.